Geophysical Journal International

Geophys. J. Int. (2011) **186,** 349–358 doi: 10.1111/j.1365-246X.2011.05034.x

Finding a realistic velocity distribution based on iterating forward modelling and tomographic inversion

Ivan Koulakov,[1] Heidrun Kopp[2] and Tatiana Stupina[1]

[1] *Institute of Petroleum Geology and Geophysics, SB RAS, Prospekt Akademika Koptuga,* 3, *Novosibirsk* 630090, *Russia. E-mail: KoulakovIY@ipgg.nsc.ru*
[2] *IFM-GEOMAR, Leibniz Institute of Marine Sciences, Wischhofstr.* 1-3, 24148 *Kiel, Germany*

Accepted 2011 April 3. Received 2011 April 3; in original form 2010 September 29

SUMMARY

Tomography is like a photograph that was taken by a camera with blurred and defective lenses that deform the shapes and colours of objects. Reporting quantitative parameters derived from tomographic inversion is not always adequate because tomographic results are often strongly biased. To quantify the results of tomographic inversion, we propose a forward modelling and tomographic inversion (FM&TI) approach that aims to find a more realistic solution than conventional tomographic inversion. The FM&TI scheme is based on the assumption that if two tomograms derived from the inversion of observed and synthetic data are identical, the synthetic structure may appear to be closer to the real unknown structure in the ground than the inversion result. However, the manual design of the synthetic velocity distribution is usually time-consuming and ambiguous. In this study, we propose an approach that automatically searches for a probabilistic model. In this approach, a synthetic model is iteratively updated while taking into account the bias of the model in previous stages of the FM&TI performance. Here, we present an example of synthetic modelling and real data processing for an active source refraction data set corresponding to a marine profile across the subduction zone in Chile at about 32°S latitude. A key feature of the model is a low-velocity channel above the subducted oceanic crust, which was defined in the synthetic model and expected in the real case. The conventional first arrival traveltime tomography was barely able to resolve this channel. However, after several iterations of the FM&TI modelling, we succeeded in reconstructing this channel clearly. In the paper, we briefly discuss the nature of this low-velocity subduction channel, and we compare the results with other studies.

Key words: Controlled source seismology; Seismic tomography; Wave propagation; Subduction zone processes.

INTRODUCTION

Traveltime seismic tomography (we call it in the paper conventional tomography) is a method, which is widely used in different basic and applied studies on scales from first metres to the entire Earth. Tomographic inversion is like a photograph that was taken by a camera with blurred and defective lenses that deform the shapes and colours of objects. Some of basic reasons for the bias in the solutions in tomographic inversion are listed below.

1. In most seismic tomographic studies, the illumination of the studied objects suffers from incomplete angular coverage, which causes smearing and biases the retrieved anomalies (e.g. Nielsen & Jacobsen 1996).
2. The amplitudes of the seismic anomalies computed in tomographic inversion are usually difficult to estimate unambiguously. If the data are noisy, the solution should be stabilized by increasing the damping in the inversion (e.g. Nolet 1985). The damping causes a decrease in the amplitude of the solution, and it may appear much lower than in reality (e.g. Trampert & van der Hilst 2005).
3. Due to inhomogeneous ray coverage, one damping value can cause over- and underestimated amplitudes in different parts of the study area (e.g. Trampert & Snieder 1996).
4. The inversion is based on rays with unknown paths, which depend on an unknown velocity distribution. This causes non-linearity, which may also affect the solution (e.g. Nolet 1987). Low-velocity anomalies, in particular, are usually underestimated because seismic rays tend to avoid them, while high-velocity patterns appear to be larger than in reality (e.g. Spakman 1993).
5. First arrival traveltime tomography usually provides continuous velocity–depth distributions, while in nature, major velocity changes often occur on first-order interfaces.

These fundamental problems exist in any seismic tomographic study to a larger or smaller extent regardless of the algorithm used. Because of these and other problems, reporting quantitative

parameters derived from tomographic inversion is usually not adequate. To quantify the results of tomographic inversion, Koulakov *et al*. (2010) proposed searching for a realistic solution based on a forward modelling and tomographic inversion (FM&TI) approach. This approach attempts to investigate the properties of the tomographic operator and to derive estimates for the quantitative values of true structures. According to the FM&TI approach, a synthetic model of a realistic configuration is created, and synthetic traveltimes are computed in the model based on the actual ray configuration. These synthetic data are then inverted using identical inversion parameters and a starting model, as in the case of real data inversion. If the reconstructed velocity distribution is similar to the result of the real data inversion, the synthetic model is closer to reality than the inversion results. Koulakov *et al*. (2010) illustrated this approach with different synthetic and real active source data sets with first arrival times. This approach has also been used in passive source studies on local (e.g. Koulakov *et al*. 2009a) and regional (e.g. Koulakov *et al*. 2009b) scales and for teleseismic studies (e.g. Koulakov *et al*. 2006).

The major problem presented by FM&TI is how to construct the synthetic model. We provided a tool within the PROFIT code (Koulakov *et al*. 2010), which allows the construction of various models of any complexity using a set of polygons and polylines. However, we admit that the process of the model design depends on the experience of the researcher, and it is rather time consuming. The ambiguity of the model construction makes a practical realization of FM&TI problematic. This study provides an automatic determination of the probabilistic velocity distribution based on an iterative FM&TI procedure.

This approach will be illustrated using synthetic data corresponding to a deep seismic sounding offshore profile in Chile at 32°S latitude. We will show that our new scheme allows the retrieval of important features that are essential for a geodynamical interpretation and that were not visible after conventional tomographic processing of first arrival times.

FM&TI APPROACH

The FM&TI scheme is based on an assumption that if two tomograms derived from an inversion of observed and synthetic data are identical, the known synthetic structure should be similar to the unknown structure in the real Earth. Koulakov *et al*. (2010) provided several examples of the realization of this scheme for different real and synthetic models. They manually adjusted synthetic models defined by a set of polygons and lines to achieve the maximum similarity between reconstructed real and synthetic models. However, this procedure is fairly time consuming, it strongly depends on the subjectivism of the researcher who designs the model, and it does not always provide a satisfactory solution.

Here, we propose a way to make this procedure automatic. We present an algorithm that is based on an iterative automatic adjustment of a synthetic model as schematically illustrated in Fig. 1. At the initial stage, we perform the inversion of real data using a tomographic code. When performing the tomographic inversion, we look for optimal starting velocities, which provide minimum time residuals and estimate reasonable values for the damping parameters. In the first stage of FM&TI, we take the result of the real data inversion (R_{real}) as a synthetic model (M_1). Then we compute the synthetic traveltimes and perturb them with realistic noise. Note that the basic assumption of the FM&TI approach is valid only if the synthetic noise is adequate and it provides same variance reduction in the real and synthetic cases For these synthetic data we perform a full tomographic inversion using the exact same parameters and the same reference model as in the case of a real data inversion. At this stage, we can estimate the properties of the tomography operator and how it biases the solution. In a scheme presented in Fig. 1, the anomaly of 10 per cent is reduced to 7 per cent and –7 per cent is reduced to –4 per cent. These values are lower than in the real data result, R_{real}. Thus, the perturbations in the synthetic model should be increased. According to this assumption, the synthetic model in the second iteration, M_2, is computed as:

$$M_2 = M_1 + (R_{\mathrm{real}} - R_1). \quad (1)$$

At the second stage, the anomalies with amplitudes of 13 and –10 per cent are reconstructed as 9.5 per cent and –7.5 per cent, which appear to be closer to R_{real}. For the next iterations (n), we update the synthetic model as:

$$M_n = M_{n-1} + (R_{\mathrm{real}} - R_{n-1}). \quad (2)$$

Normally, this procedure should converge to a model for which the reconstruction, R_n, is identical to R_{real}. When the norm of $R_{\mathrm{real}} - R_n$ becomes smaller than a predefined value, we can stop our iterations. However, in practice this scheme may fail, for example, when the damping is insufficient. In this case, we recommend increasing the inversion damping.

To perform the tomographic inversions and ray tracing in this study, we use the *PROFIT* code, which is freely available online (www.ivan-art.com/science/PROFIT). This code is described in detail in Koulakov *et al*. (2010) and in supporting text materials provided together with the online version of the code. The FM&TI scheme can be easily programmed and implemented for any other existing tomography code.

SYNTHETIC MODELLING

We designed a synthetic model (shown in Fig. 2) that represents a realistic situation corresponding to the Chilean subduction zone. In this model, a key feature is a low-velocity channel in the coupling zone between the subducting slab and the overriding plate with velocities varied from 4 to 4.87 km s^{-1}. This object is fairly difficult to detect by seismic tomography because seismic rays avoid this sharp low-velocity anomaly, and they do not provide much information about it. As will be shown, a conventional tomographic inversion, though iteratively non-linear, is unable to provide a clear image for this feature.

The source-receiver pairs for the synthetic data set and bathymetry are taken from a real active source experiment (2545 traveltimes), which is described in next section and in a separate paper by Kopp *et al*. (in preparation). The synthetic traveltimes were computed by the bending ray tracing algorithm, which is part of the PROFIT code (Koulakov *et al*. 2010). The ray paths corresponding to the 1/3 subset of the entire data used for modelling are presented in the lower plot in Fig. 2. After computing the synthetic data set, the 'true' model was 'forgotten', and these data were processed in exactly the same way as the observed data of a real experiment.

The synthetic traveltimes were perturbed with noise. In cases of active seismic schemes with densely distributed sources, the traveltimes are picked along the entire phase branches in the wave field. Therefore if there is any phase misidentification in real data processing, similar picking error may take place in several neighbouring traces. In this case, applying randomly distributed errors to each individual traveltime, as in cases of passive schemes, is not appropriate. In our algorithm, the noise is randomly generated for each

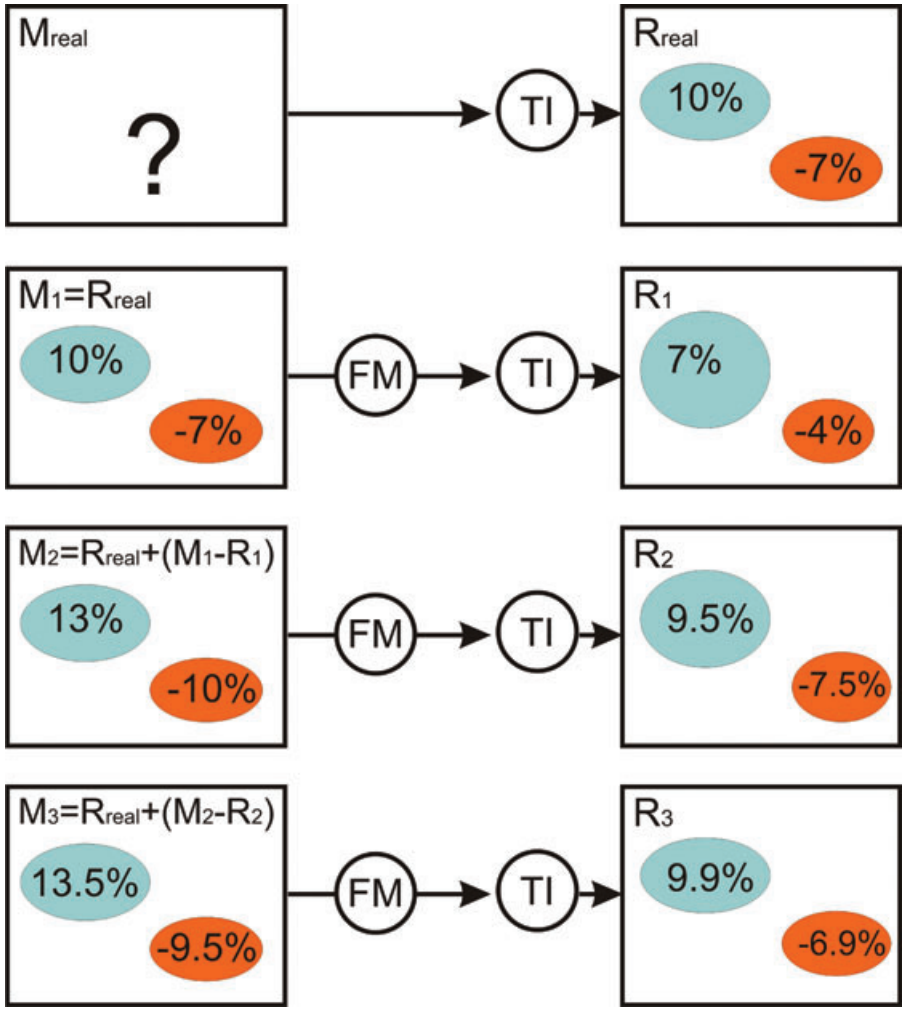

Figure 1. Schematic representation of the iterative FM&TI approach. FM is forward modelling (ray tracing); and TI is tomographic inversion. The percentages in the 'blue' and 'red' patterns are hypothetical examples of seismic anomaly amplitudes that are given to facilitate the explanation of the algorithm in the text.

of N successive picks (N is a predefined interval which reflects the coherency of data). Between these picks the values of noise are computed by linear interpolation. The basic noise values correspond to a predefined statistical distribution (e.g. Gaussian 'hat') with a predefined average value. For the presented synthetic model we applied the interval, $N = 10$, and average noise equal to 0.05 s. The maximal outlier in the data set reached 0.3 s.

The results of the iterative FM&TI processing are shown in Fig. 3. The upper row corresponds to the initial stage of the conventional tomographic inversion of 'real data' (i.e. the synthetic data for which the true model was 'forgotten') by the iterative tomographic code PROFIT. At this stage, we performed several trials with different starting models and inversion parameters to achieve the best data fit. We paid special attention to tuning the coefficients of amplitude damping and smoothing. For the best model they were equal to $W_{am} = 0.8$ and $W_{sm} = 1.0$. The estimated 2-D starting model is presented in Plot A0. The resulting velocity distribution after five iterations of conventional tomographic inversion is shown in Plot A2. As can be seen in this model, we see hardly any presence of the low-velocity channel, which is probably caused by insufficient ray coverage and non-linear effects.

At first stage of FM&TI, we take the result of 'real' data inversion as a synthetic model (Plot B1). We compute the synthetic traveltimes using a 2-D bending algorithm and perturb them with synthetic noise with 0.05 s of average magnitude. Then we perform the inversion with the identical parameters and reference model as in the case of the 'real' inversion. The result of the reconstruction, which are shown in Plot B1, appears to be smoother than the 'real' data result. Furthermore, as seen in Plot C1, when representing the difference of the reconstruction results in 'real' (Plot B0) and 'synthetic' (Plot B1) cases, the retrieved anomalies are strongly biased. This bias characterizes the properties of the tomographic operator (the photo camera with deformed lenses), which can be then used to correct the solution. The standard deviation of the differential model after the first FM&TI stage is 0.07347 km s^{-1} (Table 1).

In the next stage, we create a new synthetic model (Plot A2) using formula (2), and we again repeat the forward modelling and inversion. We see that at this stage the difference between Plots B0 and B2 is smaller than in the first iteration (see Table 1). These stages are performed iteratively several times. We see that in each stage, the difference gradually increases. In the fifth and final stage, the reconstruction (Plot B5) is almost identical to the 'real' data inversion (Plot B0), which means that the synthetic model in Plot A5 may adequately represent the 'real' velocity distribution in the Earth. The standard deviation of the differential model after the fifth FM&TI stage is 0.03211 km s^{-1}.

Next, we can compare the derived velocity distributions with the true model shown in Fig. 2. We see that after five FM&TI stages,

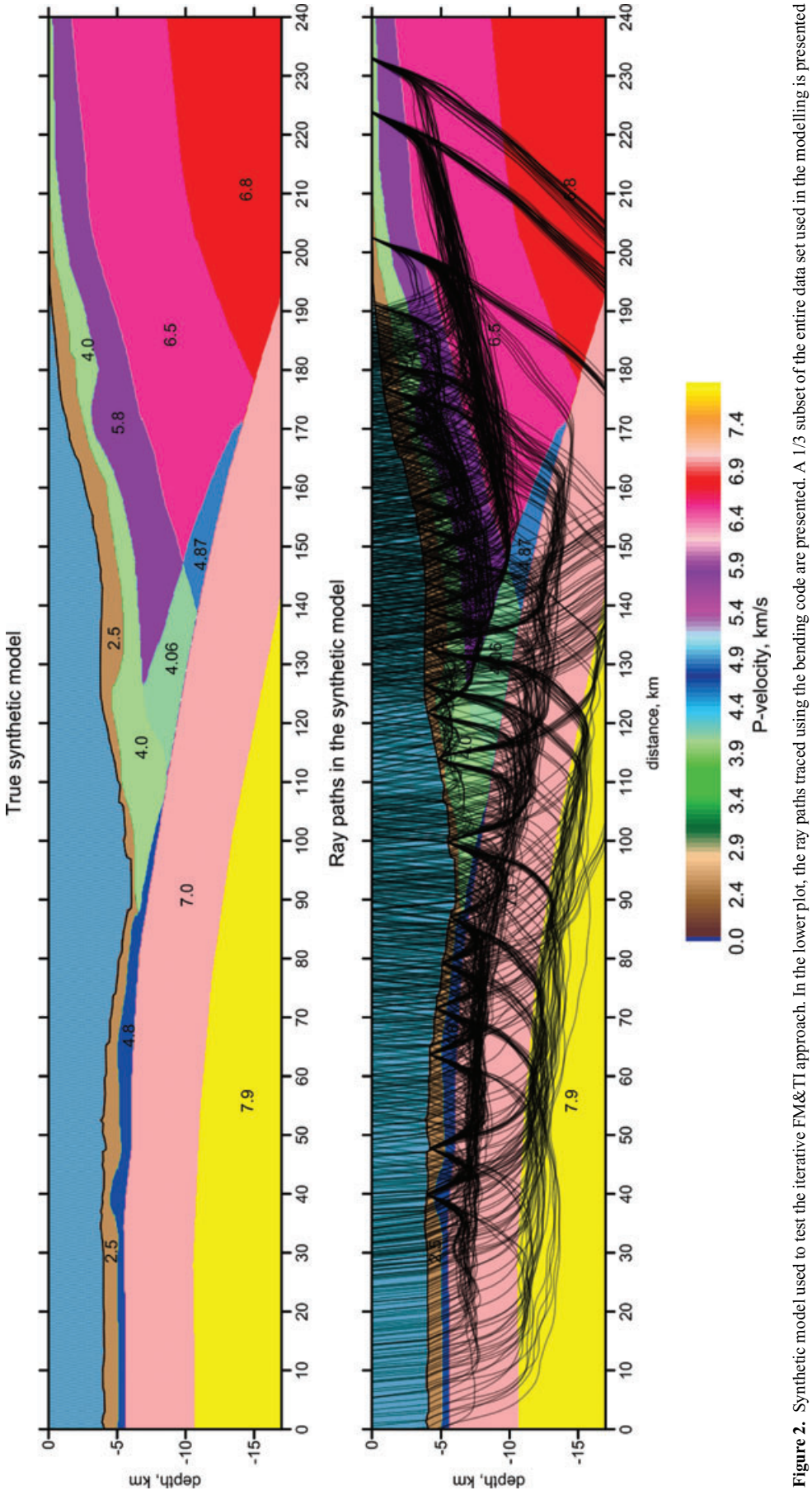

Figure 2. Synthetic model used to test the iterative FM&TI approach. In the lower plot, the ray paths traced using the bending code are presented. A 1/3 subset of the entire data set used in the modelling is presented in this plot.

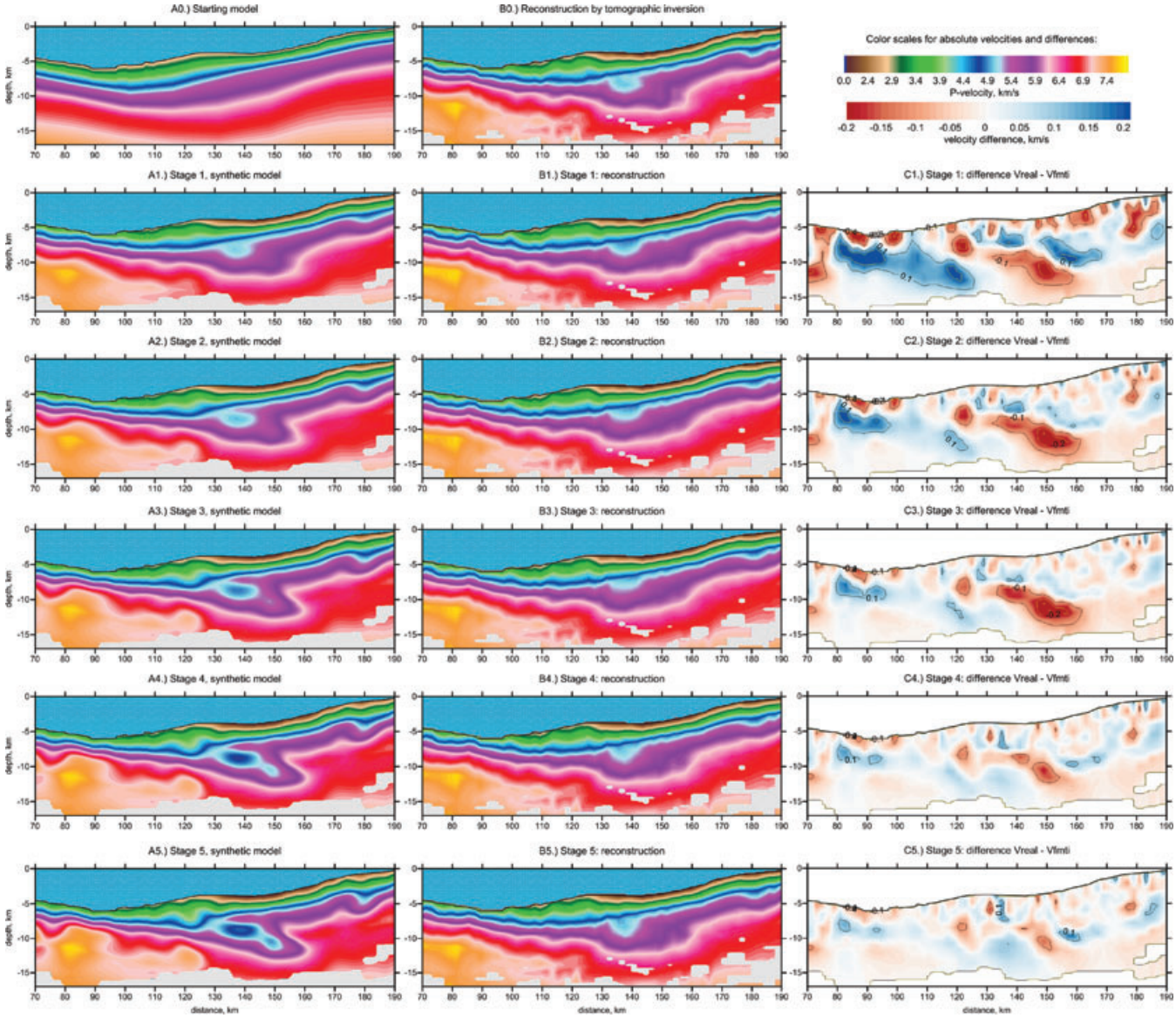

Figure 3. Stages of the iterative FM&TI reconstruction of the synthetic model presented in Figure 2. The upper row corresponds to the conventional tomographic inversion: A0 is the starting model, B0 is the result of tomographic inversion. The other plots represent the first to fifth stages of the FM&TI modelling. Plots in left column (A1–A5) represent synthetic models in the corresponding FM&TI stages; plots in central column (B1–B5) are the tomographic reconstructions of these models; and plots in right column (C1–C5) are the differences between these reconstructions and the 'real' data inversion (plot B0).

Table 1. Standard deviation of the velocity model differences (in km s^{-1}) corresponding to column C in Figs 3 and 4

FM&TI iterations	1	2	3	4	5
Synthetic model in Fig. 3	0.07347	0.05237	0.04362	0.03812	0.03211
Real model in Fig. 4	0.08599	0.06085	0.05304	0.04526	0.04070

the model in Plot A5 clearly reveals the location of the low-velocity body in the subduction channel that was not seen in the result of the conventional tomographic inversion (Plot B0). This test shows that the FM&TI approach retrieves structures more accurately than conventional tomography and that it can be used to process real observations.

REAL DATA PROCESSING

In this paper, which is mainly oriented toward presenting a new methodology, we show only one example of real data processing. Here, we consider a data set that corresponds to the offshore active source profiling experiment performed across the subduction zone in Chile at a latitude of about 32° S. The data from the airgun shots on the surface of the sea along the profile were recorded by 21 bottom seismometers and three land seismic stations. In total, we used nearly 3000 picks. The configuration of rays corresponding to these source–receiver pairs is shown in Fig. 2. Further details about the experiment conditions can be found in Kopp *et al*. (in preparation).

For the real data, we performed the same procedure, which is described in previous section, for the reconstruction of the synthetic model. The results of the modelling for this case are shown in Fig. 4.

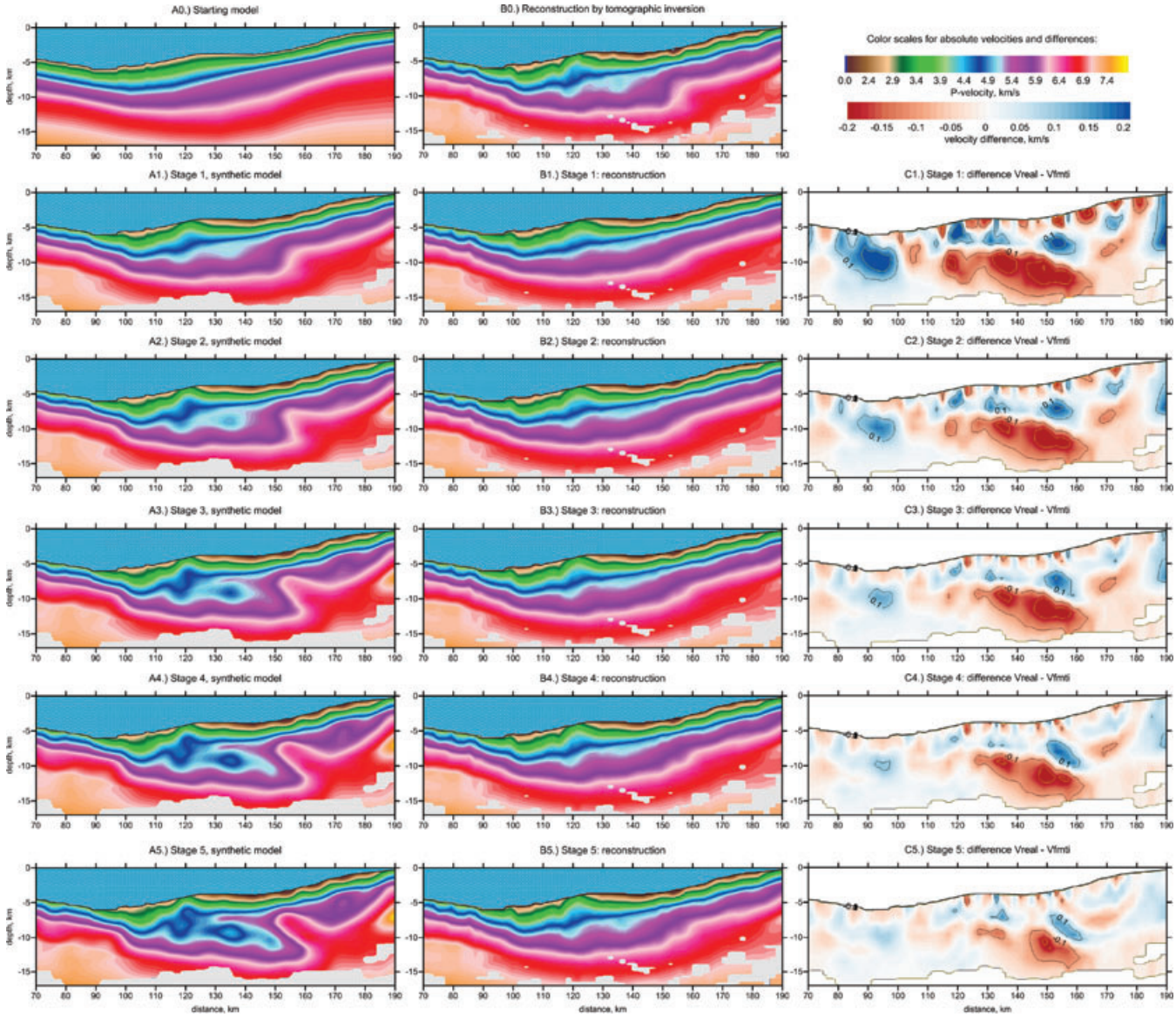

Figure 4. Stages of iterative FM&TI processing of a real data set corresponding to an active source refraction seismic profile in central Chile. The upper row corresponds to the conventional tomographic inversion. The plots in rows B, C and D represent the first, second and fifth stages of the FM&TI modelling. Plots B1, C1 and D1 are the synthetic model at the corresponding iterations; plots B2, C2 and D2 are the tomographic reconstructions of these models; and plots B3, C3 and D3 are the differences between these reconstructions and the real data inversion (plot A2).

At the initial step of the conventional tomographic inversion, we obtained a model (Plot B0) that was rather typical for these kinds of sections across the subduction zone. Similar to a number of previous studies (e.g. Sallares & Ranero 2005), we observed the high velocity plate with relatively thin crust without any sedimentary cover in the oceanic side of the section. In the continental part, we observed a thicker crust covered with sediments. Just behind the trench, we see a large low-velocity body, which corresponds to the accretionary wedge. However, almost no signature of a low-velocity subduction channel is seen in the result of the conventional tomography inversion.

These data were additionally processed according to the iterative FM&TI approach. The results of the first to fifth stages are shown in rows 2–6 in Fig. 4. It is seen that in first iteration, the resulting model (Plot B1) was strongly biased in respect to real data result (Plot B0). The maximal difference, which can be seen in Plot C1 reached 0.3 km s^{-1} and more. However, this difference gradually decreased in next stages. As seen in Table 1, standard deviation of the differential model reduces from 0.8599 to 0.04070 km s^{-1}. After five FM&TI stages, the model converged to the distribution that is shown in Plot B5. The reconstruction result appears to be close to the real data result (see the differences in Plot C5).

To explore the effect of the starting model upon the result of tomographic inversion and FM&TI modelling we performed the same steps based on other reference models. Fig. 5 shows the result for the 1-D starting model presented in Plot A. The result of tomographic inversion (Plot B) can be compared with the corresponding result in the main model (Fig. 4, Plot B0). We see that in the central part where the ray coverage is rather good these models are similar. The major difference is observed in the right side of the model where rays from different stations do not cross each other, and the final velocity seems to be strongly affected by the starting model. Partly

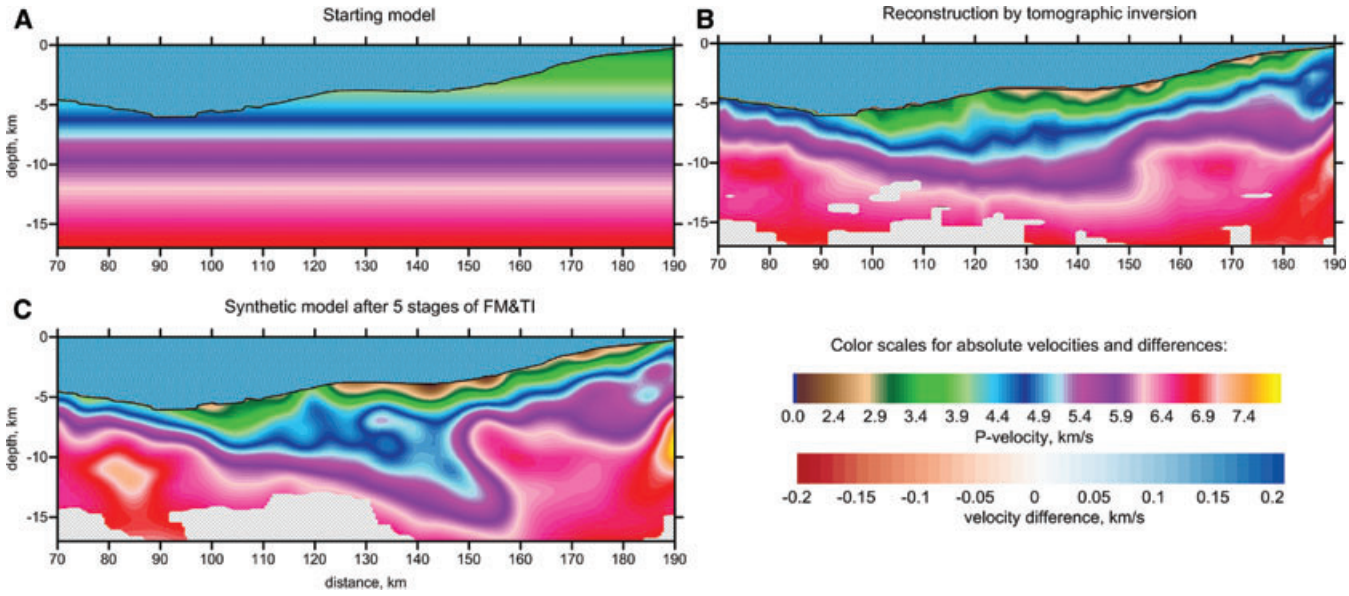

Figure 5. Results of tomographic inversion and FM&TI modelling for the 1-D starting model for real data, same as presented in Fig. 4. Panel (a) is the starting velocity distribution; panel (b) is the result of tomographic inversion and panel (c) is the best synthetic model obtained after five stages of FM&TI modelling.

this problem was solved after the iterative FM&TI modelling. The model obtained after five FM&TI steps based on the 1-D model is shown in Fig. 5(c). It can be compared with the corresponding result based on the best 2-D reference model shown in Fig. 4, Plot A5. We see that the main patterns including low-velocity anomaly above the subducting plate are reconstructed similarly in both cases. This test shows that this approach is fairly robust toward the changes in the reference model.

When performing the FM&TI modelling, the synthetic times are perturbed with random noise. The algorithm of the noise definition is described in previous section. It is important that the noise values change continuously along the traveltime curves along some segments of fixed length. We can control the coherency of noise (length of segments) and its average magnitude. In Fig. 6 we present curves of standard deviations of the residuals for tomographic inversions of real and corresponding synthetic data with different starting models, damping coefficients and noise level. Zero iteration corresponds to tracing in the starting model, while fourth iteration represents the tracing result in the velocity model after the fourth iteration (after inversion in the final fifth iteration, the ray tracing was not performed).

The values of standard deviations of the residuals for the cases of real data inversions with the 2-D and 1-D starting models (same as shown in Figs 4 and 5) are represented in Fig. 6 by solid green and violet lines. It can be seen that initially the 1-D model provides almost 1.5 times larger residuals than the starting 2-D model. However, after two iterations, the differences between the residual misfits become much smaller. In further iterations this difference remains almost unchanged. This test shows that, although the 1-D and 2-D models provide similar inversion results, the using of the 2-D model is more preferable as it enables better data fit at the initial and final stages.

The effect of damping was explored for the inversion with the 2-D starting model. The variance reductions corresponding to stronger and weaker damping values are represented by red and green curves in Fig. 6. In this cases we change similarly the coefficients for amplitude damping ($W_{am} = 1.6$ and $W_{am} = 2.2$) and smoothing ($W_{sm} = 1.6$ and $W_{sm} = 2.2$). It can be seen that the inversion with

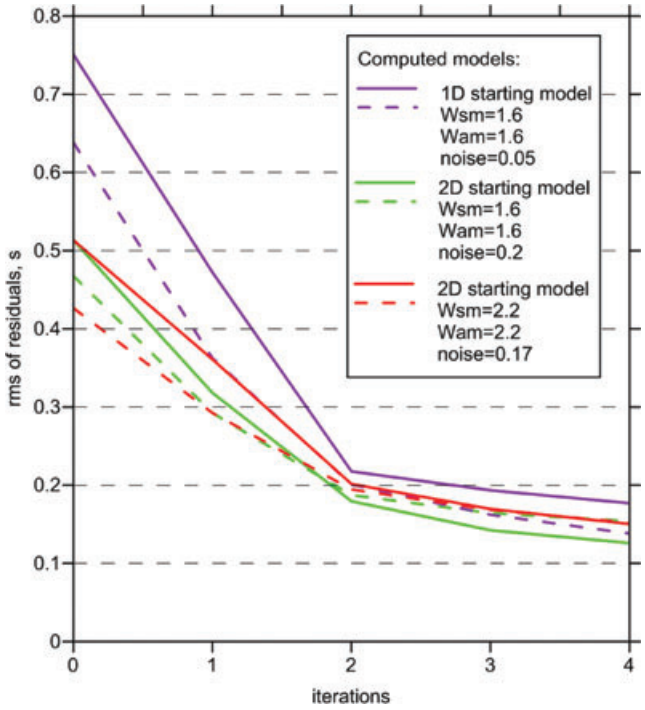

Figure 6. Values of standard deviation of residuals during four iterations of tomographic inversion for real data (solid lines) and corresponding synthetic models estimated after five FM&TI stages (dotted line). Zero iteration corresponds to the results of tracing in starting models. Different colours represent examples of three trials with different starting models, noise levels and damping coefficients (the corresponding values are given in inset).

smaller damping (green solid curve) leads faster to the solution with smaller misfit. At the same time, we found that the similar solutions are obtained for the cases of weak damping with fewer numbers of iterations and for strong damping with many iterations. As these parameters affect similarly the solutions, in most our trials we fixed the number of iterations at five (as a compromise between

calculation speed and reduction of the non-linear effect) and tuned the properties of the solution by the damping coefficients.

When performing the FM&TI modelling it is important to apply the realistic noise so that the curves of the residual norms appear to be similar in cases of real and synthetic data inversions. Dotted lines in Fig. 6 represent variance reduction curves for different synthetic models obtained after five FM&TI stages. In these cases the level of noise was different. For the case of the 1-D starting model (violet lines) the average noise magnitude was equal to 0.05 s. Looking at the curve of the residual standard deviation, we see that this value appears to be underestimated: the final data fit for the synthetic model is about 0.04 s smaller than in the case of real data. For the case of 2-D starting model with strong damping (red lines), the noise 0.17 s magnitude looks appropriate, as providing the best fit in the final iteration. However, in first iterations the misfit between synthetic and real data is rather large. We prefer the noise 0.2 s which provides the minimal misfit along the entire variance reduction curve in all iterations for the models depicted by green lines. This case is presented as the main result of this study in Fig. 4.

For the presented profile, we claim that the synthetic model obtained after five FM&TI stages shown in Plot A5 in Fig. 4 was more realistic than the result of the real data inversion shown in Plot B0. In further discussions, we will use these synthetic models as the main results of our tomographic modelling. In this resulting model, we observe rather clearly the presence of a low-velocity channel that dips along the subducting plate. The velocity inside this channel is about 4.4–4.9 km s^{-1} while in the overlying layer it reaches 5.4 km s^{-1}. A quite similar feature was obtained in the synthetic modelling shown in Fig. 3.

DISCUSSION

Advantages and problems of the FM&TI approach

In the case to conventional tomographic inversion the forward operator, F, transforms the space of the model, M, to the space of traveltimes T: $F(M) = T$. The spaces M and T are different in dimensions and properties, and the transformation F is rather complex. For example, a time anomaly can be attributed to velocity variations in the model in any place around the corresponding ray path. In a case of incomplete ray coverage, the inverse operator F^{-1} appears to be poorly determined and ill-posed (e.g. Tikhonov & Arsenin 1979).

The FM&TI optimization is based on an operator G which transforms the model space $M1$ to another model space $M2$: $G(M1) = M2$. It is important that these two spaces have the same dimensions and similar properties. In particular, we can predict that changes in one point of $M1$ will probably cause proportional changes in the same location of the $M2$ space. This make the modelling results more robust than in the case of tomographic inversion.

At the same time, we should keep in mind that the problem of non-uniqueness may appear rather serious in the case of G^{-1}-operator, similarly as well known non-uniqueness for the F^{-1} operator (e.g. Deal & Nolet 1996). If we further continue the FM&TI stages, the reconstruction results remain unchanged while the amplitudes of patterns in the synthetic models may vary to a great extent, especially for small-scale and marginal patterns. In a case if $G(M1 + \Delta M1) \sim G(M1)$, the variation $\Delta M1$ is in the null-space and it cannot be resolved by the inverse operator. This problem is seen in results of FM&TI modelling for the real data (Fig. 4). We stop our calculations after fifth stage, although the difference between the reconstructed models (Plot C5) is still considerable. When we further continue the calculations, this difference does not change anymore. The synthetic model becomes more and more heterogeneous, while the reconstruction result remains unchanged. It means that these anomalies are in the null-space, and changing the model to their values produces equivalent models for the G operator. The problem of the null-space equivalence should be taken into account when defining the number of the FM&TI stages: while updating the model does not cause any change in differential model, the calculations should stop.

Similar problem of the non-uniqueness takes place while using the inverse tomographic operator $M = F^{-1}(T)$. The advantage of the FM&TI approach compared to conventional tomography is that it indicates exactly the location of the model null-space features, for which changes of the model $M1$ does not cause any changes in $M2$. The results in these areas should be interpreted with prudence. In our case it means that the low-velocity anomaly in the subduction channel below 10 km depth at 140–150 km distance is not resolved robustly. We see that this feature is resolved differently in two presented trials in Figs 4 and 5.

Interpretation of the resulting model

Although this paper is rather methodological, we would like to provide short discussion on the nature of the discovered structures along the considered profile in Chile at about 32° latitude. The obtained low velocity anomaly can be explained by the presence of a channel in the contact between the subducting oceanic lithosphere and the overriding plate which has been actively discussed in many different studies. Scholl *et al*., (1977) gave the definition of the subduction channel as a poorly consolidated, fluid-rich layer that is structurally squeezed between upper and lower plates in subduction zones. Similar definitions were given in other later studies supported by different geophysical observations (e.g. Shreve & Cloos 1986). The subduction channel is constituted by the oceanic and continental sediments cumulated in the trench that are dragged with the downgoing plate beneath the margin. It can also include debris from the overriding plate. A good description of the seismic characterization of a subduction channel in South America can be found in Calahorrano *et al*. (2008).

There is much evidence for the existence of this strongly deformed zone beneath northern Andes based on geological (e.g. Vannucchi *et al*. 2008) and geophysical observations (e.g. Sallares & Ranero 2005; Ranero & von Huene 2000) and numerical (e.g. Babeyko & Sobolev 2008) and physical modelling (e.g. Kukowski & Onken 2006). The existence of fluids in this channel is considered one of the major parameters that control the processes in subduction zones (e.g. Le Pichon *et al*. 1993). Another Chilean profile, at about 23.5°S latitude, was investigated by Von Huene & Ranero (2003) and Sallares & Ranero (2005). These researchers discovered the presence of high relief horst and graben structures on the top of the subducting oceanic crust. These structures are assumed to generate a strong abrasion and erosion of the overriding plate. Tectonic erosion removes material from the overriding plate and inputs it into the subduction channel. The subduction erosion determines the properties of the subduction channel and the regime of the entire subduction system. This is a fundamental process in sediment-starved margins. Basal erosion has been frequently associated to hydrofracturing of the base of the overriding plate by fluids released from the subduction channel and the subducting crust (e.g. von Huene & Ranero 2003; Sallarès & Ranero 2005). The trench axis along the Chilean margin contains little detectable sediment, which is an important

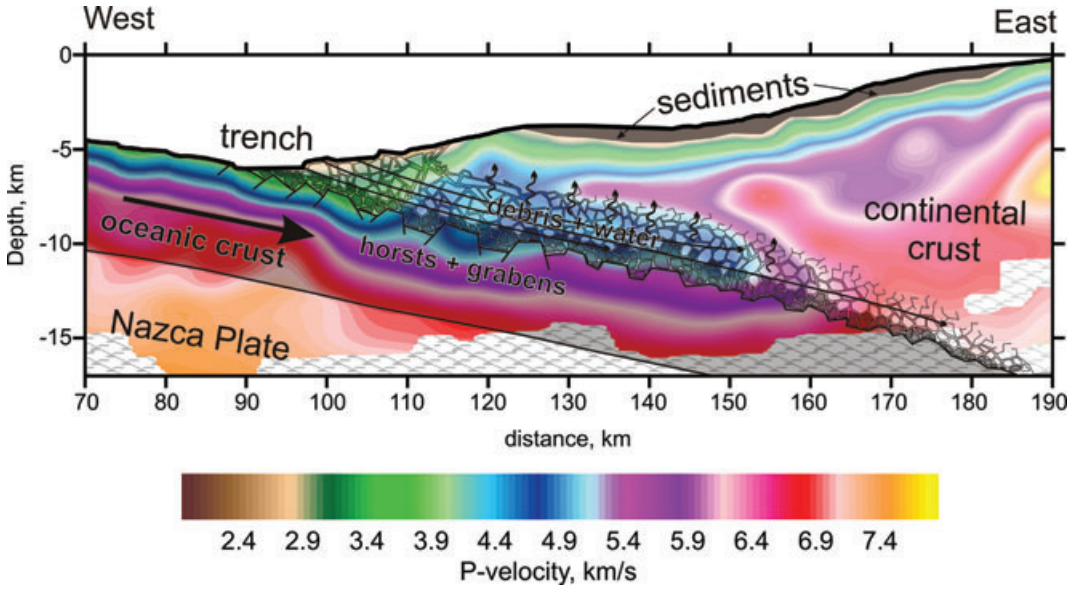

Figure 7. Schematic interpretation of the velocity profile across the subduction zone in Chile at about 32°S. Background is the velocity structure derived in this study (Plot D1 in Fig. 4). Oceanic crust with originated from it debris is depicted by darker colour; overriding plate with corresponding debris is lighter. Black arrows indicate migration of water along the subduction channel and its upward escape.

factor for very high friction rates in the subduction channel. These factors have to intensify the erosion process.

We propose that a similar situation as for the profile studied by Sallares & Ranero (2005) takes place for the case considered in this study. A schematic interpretation of our velocity model is presented in Fig. 7. We believe that the oceanic crust is strongly perturbed by horst and graben structures, similarly to the case considered by Sallares & Ranero (2005). Due to the lack of sediments in the trench and a very high friction rate, the moving oceanic crust destroys the overriding plate and is sheared off by itself. The debris originating from the disintegration of the overriding and oceanic plates forms a weakened zone along the subduction coupling. The thickness of this layer is estimated to be about 1.5 km (Von Huene & Ranero 2003), although the upper limit of the disintegration zone is barely detectable in reflection and refraction seismic studies. Von Huene & Ranero (2003) claimed that this debris material in the subduction channel includes about 30 per cent pores, which may entrain ocean water downward along the subduction. Some of this water may escape upward to the overriding continental crust, as shown by the small arrows in Fig. 7.

Our model generally supports this scenario. We clearly see the elongated low-velocity pattern, which can be interpreted as the subduction channel filled with water-rich debris. However, in our model, this channel seems to be thicker than what has been estimated by other authors who claim that thickness of this layer may vary from a few hundreds of meters to a few kilometres (e.g. Von Huene & Ranero 2003, Calahorrano *et al*. 2008). There may be several reasons for such inconsistency. First, as was previously mentioned, the upper limit of the subduction channel is difficult to detect by seismic methods because the disintegration in the overriding plate may occur in a continuous zone without clear limits. Second, this channel may appear thicker because of the upward migration of fluids from the channel to the overriding plate, which should also cause a decrease in velocity. Third, as we see in synthetic modelling, the algorithm does not have enough resolution to resolve 1.5-km-thick patterns, making it look smeared and thicker in the resulting images. To conclude this discussion, we claim that our result is generally supported by the available information on the structure of subduction complexes.

CONCLUSIONS

In this study, we proposed an iterative FM&TI approach that automatically searches for a realistic model. The main conclusion of this study is that the proposed iterative FM&TI approach allows the retrieval of much more realistic structures than conventional tomographic inversion. In the presented synthetic and real data examples, we showed that only after applying several stages of the FM&TI modelling were we able to reconstruct a low-velocity subduction channel, which was barely visible in the results of the conventional tomographic inversion.

The previous version of the FM&TI approach described in Koulakov *et al*. (2010) did not provide a practical tool for constructing a probabilistic synthetic model. It was just stated that if one would be able to built a model with similar reconstruction as in the real case, this model would be close to the reality. But constructing this model was almost a matter of art. It was very ambiguous and technically difficult. In this paper we propose an approach which is very simple and automatically bring us to the probabilistic solution. The principle of this approach is rather simple and transparent, and it can be easily programmed and implemented for any existing tomography code. We propose that this approach can be used for any tomographic study at any scale for exploration, engineering and scientific purposes. In particular, we believe that it can be suitable not only for the first arrival time data sets as considered in this study, but for many other tomographic schemes including refraction/reflection schemes. It is important that any a priori information be included in the synthetic model, if available. In particular, a synthetic model can initially include known interfaces with sharp velocity contrasts.

Although this paper is rather methodological, we would like to focus the reader's attention to an exceptionally clear image of a low-velocity subduction channel obtained for the considered profile in Chile. This result is crucial for quantifying the processes in the coupling area of the upper segment of the subduction zone. In

our opinion, it is important to revisit the existing data for other subduction zones and to reprocess them using the iterative FM&TI approach. It is possible that this will reveal some important features that are not retrieved by conventional tomography inversions.

ACKNOWLEDGMENTS

Wide-angle data were acquired by IFM-GEOMAR during RV SONNE cruise SO161 supported by the BMBF. This work is supported by the Helmholtz Society and RFBR Joint Research Project 09–05-91321-SIG a, Multidisciplinary Projects SB RAS #21, SB-UrO-DVORAS #96, and Project ONZ RAS #7.4. Arrows indicate the migration of water along the subduction channel and its upward escape.

REFERENCES

Babeyko A.Y. & Sobolev, S.V., 2008. High-resolution numerical modeling of stress distribution in visco-elasto-plastic subducting slabs, *Lithos,* **103**(1–2), 205–216.

Calahorrano, A., Sallares, V., Sage, F., Collot, J-Y. & Ranero, C.R., 2008. Nonlinear variations of the physical properties along the Southern Ecuador subduction channel: results from depth-migrated seismic data. *Earth. planet. Sci. Lett.,* **267,** 453–467, doi:10.1016/j.epsl.2007.11.061.

Deal, M. & Nolet, G., 1996. Nullspace shuttles, *Geophys. J. Int.,* **124,** 372–380.

Koulakov I., Sobolev, S.V., Weber, M., Oreshin, S., Wylegalla, K. & Hofstetter, R., 2006, Teleseismic tomography reveals no signature of the Dead Sea Transform in the upper mantle structure, *Earth. planet. Sci. Lett.* **252**(1–2), 189–200.

Koulakov I., Yudistira, T., Luehr, B.-G. & Wandono, 2009a. P, S velocity and VP/VS ratio beneath the Toba caldera complex (Northern Sumatra) from local earthquake tomography, *Geophys. J. Int.,* **177,** 1121–1139, doi:10.1111/j.1365–246X.2009.04114.x.

Koulakov I., Kaban, M.K., Tesauro, M. & Cloetingh, S., 2009b. P and S velocity anomalies in the upper mantle beneath Europe from tomographic inversion of ISC data, *Geophys. J. Int.* **179**(1) 345–366, doi:10.1111/j.1365–246X.2009.04279.x.

Koulakov I., Stupina, T. & Kopp, H., 2010. Creating realistic models based on combined forward modeling and tomographic inversion of seismic profiling data, *Geophysics,* **75**(3), B115, doi:10.1190/1.3427637.

Kukowski N. & Oncken, O., 2006. Subduction erosion—the "Normal" mode of fore-arc material transfer along the Chilean Margin? in *The Andes—Active Subduction Orogeny,* Vol. 1, Front Earth Sci. Ser., pp. 217–236, eds Oncken, O., Chong, G., Franz, G., Giese, P., Goetze, H-J., Ramos, V.A., Strecker, M.R. & Wigger, P., Springer-Verlag, Berlin.

Le Pichon, X.,Henry, P. & Lallemant, S., 1993. Accretion and erosion in subduction zones: the role of fluids. *Annu. Rev. Earth planet. Sci.,* **21,** 307–331.

Nielsen, L. & Jacobsen, B. H., 1996. Resolution and error propagation analysis for tomographic data with correlated errors, in *Inverse Methods, Interdisciplinary Elements of Methodology, Computation and Application,* pp. 131–138, eds Jacobsen, B. H., Mosegaard, K. & Sibani, P., Springer-Verlag, Berlin, ISBN 3–540-61693–4.

Nolet, G., 1985. Solving or resolving inadequate and noisy tomographic systems, *J. Comp. Phys.,* **61,** 463–482.

Nolet, G., 1987, Seismic wave propagation and seismic tomography, in *Seismic Tomography, With Application, in Global Seismology and Exploration Geophysics,* pp. 1–27, Reidel, Dordrecht.

Ranero, C.R. & Von Huene, R., 2000. Subduction erosion along the Middle America convergent margin. *Nature,* **404,** 748–752.

Sallarès, V. & Ranero, C.R., 2005, Structure and tectonics of the erosional convergent margin off Antofagasta, north Chile (23°30′S), *J. geophys. Res.,* **110,** B06101, doi:10.1029/2004JB003418.

Scholl, D.W., Marlow, M.S. & Cooper, A.K., 1977. Sediment subduction and offscrapping at Pacific margins, in *Island Arcs, Deep Sea Trenches, and Back-Arc Basins,* Vol. 1, Maurice Ewing Ser., pp. 199–210, eds Talwani, M., & Pitman, W.C., III, Am. geophys. Union., Washington, D.C.

Shreve, R.L. & Cloos, M., 1986. Dynamics of sediment subduction, melange formation, and prism accretion, *J. geophys. Res.,* **91**(B10), 10 299–10 245.

Spakman, W., 1993, Iterative strategies for nonlinear travel-time tomography using global earthquake data, in *Seismic Tomography: Theory and Applications,* pp. 190–226, eds Iyer, H.M. & Hirahara, K., Prentice-Hall, London.

Tikhonov, A.N. & Arsenin, V.Y., 1979. *Methods for Solving Ill-Posed Problems,* Nauka, Moscow.

Trampert J. & Snieder R., 1996. Model estimations biased by truncated expansions: possible artifacts in seismic tomography, *Science,* **271,** 1257–1260.

Trampert, J. & Van Der Hilst, R.D., 2005. Towards a quantitative interpretation of global seismic tomography, *Geophys. Monogr.,* **160,** 47–62.

Vannucchi, P., Remitti, F. & Bettelli, G., 2008. Geological record of fluid flow and seismogenesis along an erosive subducting plate boundary. *Nature,* **451,** 699–704, doi:10.1038/nature06486.

Von Huene, R. & Ranero, C. R., 2003. Subduction erosion and basal friction along the sediment-starved convergent margin off Antofagasta, Chile, *J. geophys. Res,* **108,** 2079, doi:10.1029/ 2001JB001569.